Timing and tempo of the Great Oxidation Event

Ashley P. Gumsley[a,1], Kevin R. Chamberlain[b,c], Wouter Bleeker[d], Ulf Söderlund[a,e], Michiel O. de Kock[f], Emilie R. Larsson[a], and Andrey Bekker[g,f]

[a]Department of Geology, Lund University, Lund 223 62, Sweden; [b]Department of Geology and Geophysics, University of Wyoming, Laramie, WY 82071; [c]Faculty of Geology and Geography, Tomsk State University, Tomsk 634050, Russia; [d]Geological Survey of Canada, Ottawa, ON K1A 0E8, Canada; [e]Department of Geosciences, Swedish Museum of Natural History, Stockholm 104 05, Sweden; [f]Department of Geology, University of Johannesburg, Auckland Park 2006, South Africa; and [g]Department of Earth Sciences, University of California, Riverside, CA 92521

Edited by Mark H. Thiemens, University of California, San Diego, La Jolla, CA, and approved December 27, 2016 (received for review June 11, 2016)

The first significant buildup in atmospheric oxygen, the Great Oxidation Event (GOE), began in the early Paleoproterozoic in association with global glaciations and continued until the end of the Lomagundi carbon isotope excursion ca. 2,060 Ma. The exact timing of and relationships among these events are debated because of poor age constraints and contradictory stratigraphic correlations. Here, we show that the first Paleoproterozoic global glaciation and the onset of the GOE occurred between ca. 2,460 and 2,426 Ma, ∼100 My earlier than previously estimated, based on an age of 2,426 ± 3 Ma for Ongeluk Formation magmatism from the Kaapvaal Craton of southern Africa. This age helps define a key paleomagnetic pole that positions the Kaapvaal Craton at equatorial latitudes of 11° ± 6° at this time. Furthermore, the rise of atmospheric oxygen was not monotonic, but was instead characterized by oscillations, which together with climatic instabilities may have continued over the next ∼200 My until ≤2,250–2,240 Ma. Ongeluk Formation volcanism at ca. 2,426 Ma was part of a large igneous province (LIP) and represents a waning stage in the emplacement of several temporally discrete LIPs across a large low-latitude continental landmass. These LIPs played critical, albeit complex, roles in the rise of oxygen and in both initiating and terminating global glaciations. This series of events invites comparison with the Neoproterozoic oxygen increase and Sturtian Snowball Earth glaciation, which accompanied emplacement of LIPs across supercontinent Rodinia, also positioned at low latitude.

Great Oxidation Event | Snowball Earth | Paleoproterozoic | Kaapvaal Craton | Transvaal Supergroup

The early Paleoproterozoic is characterized by dramatic changes in Earth's atmosphere and oceans, with the transition from anoxic to oxic conditions commonly referred to as the Great Oxidation Event (GOE) (1). It is generally thought that the onset of the GOE was a singular event (2), an assumption rooted in the perceived bistability of atmospheric oxygen (3). However, this inferred bistability in oxygen was challenged through additional modeling (4), allowing for multiple oscillations in atmospheric oxygen during the onset of the GOE. Geological evidence has also established that this transition was broadly coincident with emplacement of numerous large igneous provinces (LIPs) (5) on extensive continental landmasses positioned at low latitudes (6) and glaciations interpreted to reflect global Snowball Earth conditions (7). Models linking these events have been hampered, however, by uncertainties in local and global stratigraphic correlations and age constraints (2). Evidence from the Huronian Supergroup on the Superior Craton in Canada, which hosts three Paleoproterozoic glacial intervals, indicates that the GOE is bracketed in age between ca. 2,460 and 2,308 Ma (8–10). New observations from the critical Transvaal Supergroup in southern Africa indicate that the GOE may have occurred by ca. 2,310 Ma (9) but requires a fourth glaciation at ≤2,250–2,240 Ma (9, 11) before the development of the oldest widely accepted oxygenated paleosols (12) and red-bed sandstones (13). Discrepancies in correlations between these glacially influenced stratigraphic successions and the age of the GOE hinge on a disputed age for the Ongeluk Formation basalts (14–16). By using high-resolution in situ secondary ion mass spectrometry (SIMS) on microbaddeleyite grains coupled with precise isotope dilution thermal ionization mass spectrometry (ID-TIMS) and paleomagnetic studies, we resolve these uncertainties by obtaining accurate and precise ages for the volcanic Ongeluk Formation and related intrusions in South Africa. These ages lead to a more coherent global perspective on the timing and tempo of the GOE and associated global glaciations and LIPs.

Transvaal Supergroup

The Neoarchean to Paleoproterozoic Transvaal Supergroup overlies the Kaapvaal Craton and is preserved in two main subbasins. In the Griqualand West subbasin, the Makganyene Formation consists of a series of glaciomarine diamictites (Fig. 1) (17). Paleomagnetic data for the Ongeluk Formation, which conformably overlies and interfingers with the Makganyene Formation, indicate that these glacial sedimentary rocks were deposited at low latitude, implying a glacial event of global extent (6, 7). The age of the Ongeluk Formation basalts has long been accepted at 2,222 ± 13 Ma based on a whole-rock Pb-Pb isochron date (14) and correlation with the noncontiguous basalts of the ≤2,250–2,240 Ma Hekpoort Formation in the Transvaal subbasin (11, 12, 14, 18), although this correlation has been questioned recently (15, 16, 19). The Ongeluk Formation is overlain by banded iron and manganese deposits of the Hotazel Formation, which in turn, are followed by carbonate rocks of the Mooidraai Formation (Fig. 1). Pb-Pb and U-Pb dating of the Mooidraai Formation carbonates has yielded dates of 2,394 ± 26 and 2,392 ± 23 Ma (15, 20), respectively, in conflict with the 2,222 ± 13 Ma Pb-Pb date on the stratigraphically

Significance

We present U-Pb ages for the extensive Ongeluk large igneous province, a large-scale magmatic event that took place near the equator in the Paleoproterozoic Transvaal basin of southern Africa at ca. 2,426 Ma. This magmatism also dates the oldest Paleoproterozoic global glaciation and the onset of significant atmospheric oxygenation. This result forces a significant reinterpretation of the iconic Transvaal basin stratigraphy and implies that the oxygenation involved several oscillations in oxygen levels across 10^{-5} present atmospheric levels before the irreversible oxygenation of the atmosphere. Data also indicate that the Paleoproterozoic glaciations and oxygenation were ushered in by assembly of a large continental mass, extensive magmatism, and continental migration to near-equatorial latitudes, mirroring a similar chain of events in the Neoproterozoic.

Author contributions: A.P.G., U.S., and M.O.d.K. designed research; A.P.G., K.R.C., W.B., U.S., M.O.d.K., and E.R.L. performed research; K.R.C., W.B., U.S., and M.O.d.K. contributed new reagents/analytic tools; A.P.G., K.R.C., W.B., U.S., M.O.d.K., E.R.L., and A.B. analyzed data; and A.P.G., K.R.C., W.B., U.S., M.O.d.K., E.R.L., and A.B. wrote the paper.

The authors declare no conflict of interest.

This article is a PNAS Direct Submission.

Freely available online through the PNAS open access option.

[1]To whom correspondence should be addressed. Email: ashley.gumsley@geol.lu.se.

This article contains supporting information online at www.pnas.org/lookup/suppl/doi:10.1073/pnas.1608824114/-/DCSupplemental.

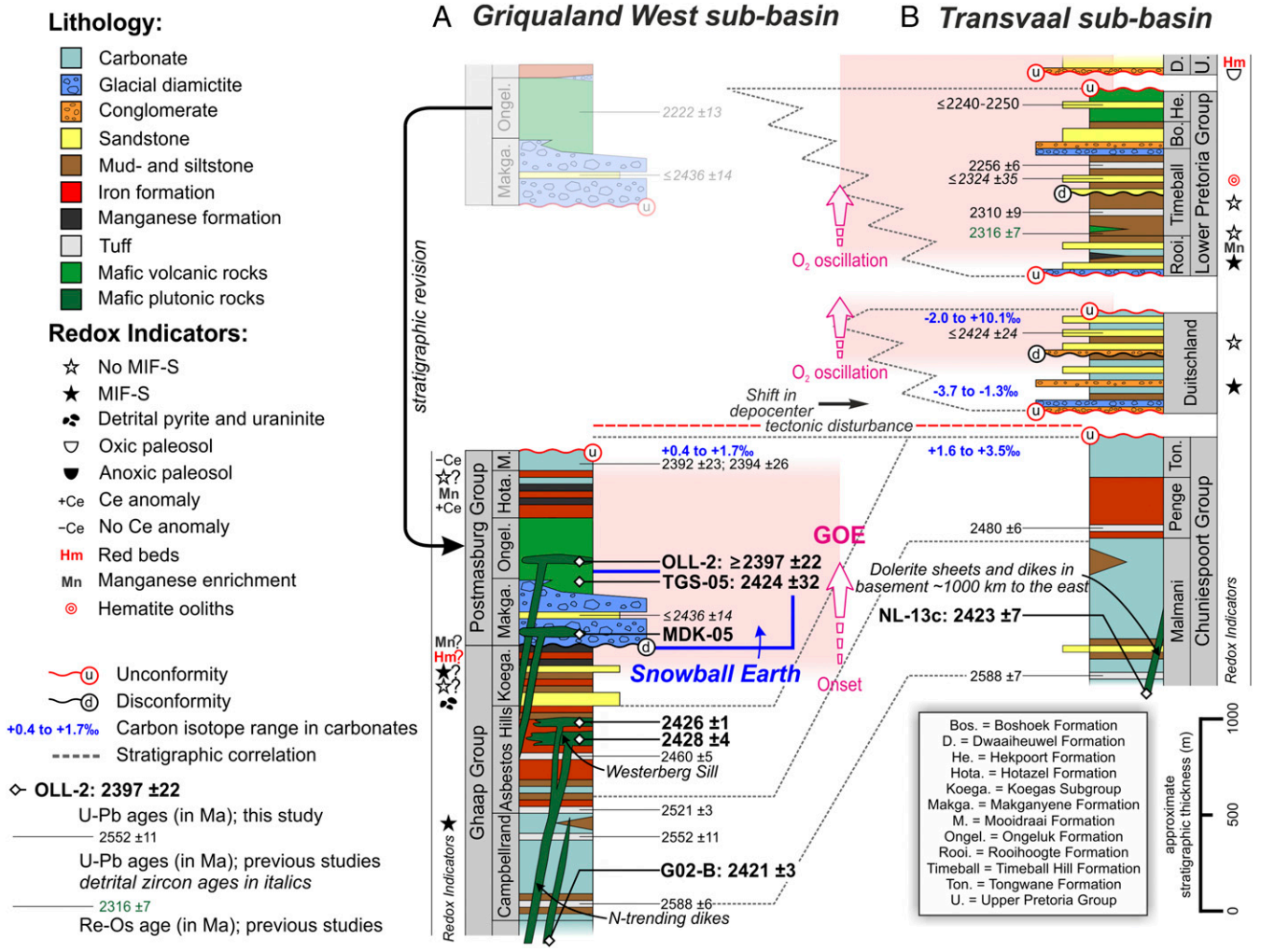

Fig. 1. Stratigraphic synthesis (*SI Methods*, *Stratigraphic Synthesis*) of the Transvaal Supergroup as preserved in its two main subbasins: (*A*) Griqualand West in the southwest and (*B*) Transvaal in the northeast. Dated samples and results (bold) are shown in stratigraphic context and collectively, unlock the long-held correlation between the basalts of the Ongeluk and Hekpoort formations (12, 14, 18). A selection of previously published ages is schematically shown (Table S1) along with redox indicators and ranges of carbon isotope values in carbonates (Table S2). The redox records within the two subbasins tracks the rhythm of GOE and reflects at least two O_2 oscillations back through 10^{-5} PAL after the onset of GOE (bold pink arrows and variable intensity pink background shading). Redox indicators requiring more detailed studies are denoted with question marks. All ages are quoted at 2σ uncertainty.

lower Ongeluk Formation (14). The Hotazel Formation hosts giant Mn deposits with a negative Ce anomaly that are unequivocally interpreted to reflect deposition after the onset of the GOE (7, 21), whereas the Koegas Subgroup underlying the Makganyene Formation contains detrital pyrite and uraninite grains signifying deposition before the GOE (22). In the Transvaal subbasin (Fig. 1), the start of the GOE has been placed in the middle of either the Duitschland Formation or the Rooihoogte Formation by different authors (23, 24), with the age of the upper Duitschland Formation constrained by detrital zircon to ≤2,424 ± 24 Ma (11). A 2,316 ± 7 Ma Re-Os age for diagenetic pyrite (25) and a 2,309 ± 9 Ma U-Pb age for tuff in the lower Timeball Hill Formation (9), which conformably overlies the Rooihoogte Formation, suggest that the GOE began by ca. 2,309 Ma (24). All chronological and redox records for the Transvaal Supergroup are provided in Tables S1 and S2.

Sampling

To test and resolve some of these critical correlations, we have dated by U-Pb isotopic methods a number of dolerite and basalt samples that are linked geologically and paleomagnetically to the Ongeluk Formation basalts (*SI Methods*, *Sampling*, Fig. S1, and Table S3). An N-trending dolerite dike from the Griqualand West subbasin (G02-B) (Fig. 1) (26) as well as an intrusive dolerite sheet from the southeastern Kaapvaal Craton (NL-13c) (Fig. 1) (27) were dated using U-Pb ID-TIMS on baddeleyite. Samples TGS-05 and OLL-2, a coarse-grained, thick basalt flow and a dolerite sill, respectively, from near the base of the Ongeluk Formation basalts (Fig. 1) (6) were dated by in situ U-Pb SIMS on microbaddeleyite grains. To couple geochronological and paleomagnetic records for these mafic units, complementary paleomagnetic studies were conducted on specimens from the TGS-05 and MDK-05 sample sites (Fig. 1) using conventional demagnetization techniques.

Results

Samples G02-B and NL-13c produce upper intercept baddeleyite dates of 2,421 ± 3 and 2,423 ± 7 Ma, respectively (Fig. 2, *SI Methods*, *Geochronology—ID-TIMS Analysis*, Fig. S2, and Table S4), whereas samples TGS-05 and OLL-2 yield upper intercept dates of 2,424 ± 32 and 2,397 ± 22 Ma, respectively (Fig. 2, *SI Methods*, *Geochronology—SIMS Analysis*, Fig. S2, and Table S5). The upper intercept dates of 2,424 ± 32, 2,423 ± 7, and 2,421 ± 3 Ma are interpreted as reliable crystallization ages and overlap within 2σ uncertainty, whereas the date obtained from OLL-2 is likely affected by a minor contribution of secondary zircon as

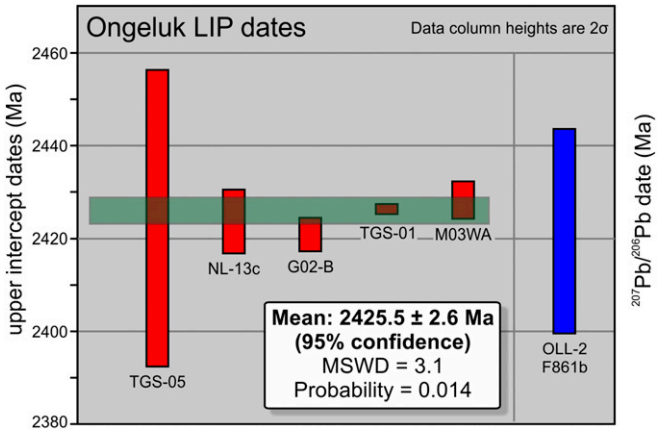

Fig. 2. Weighted mean age of the Ongeluk LIP. Shown is a comparison of upper intercept dates with 2σ uncertainties (red columns) from five samples of the Ongeluk LIP, including the Westerberg Sill Province (samples TGS-01 and M03WA) (28), with a calculated weighted mean age of 2,425.5 ± 2.6 Ma (green bar). The result from a single analysis spot (F861b in OLL-2) is shown for comparison (blue column) (Fig. S2).

indicated by SEM imaging. We, therefore, interpret the 2,397 ± 22 Ma date of OLL-2 as a minimum age. In support of this interpretation, one baddeleyite grain (spot F861b) (Fig. 2) yielded a ^{207}Pb/^{206}Pb date of 2,421 ± 22 Ma.

A structurally corrected virtual geomagnetic pole (VGP) for the dated sample TGS-05 is located at −0.7° N and 288.2° E, whereas the VGP of sample MDK-05 is located at −0.9° N and 283.7° E (*SI Methods*, *Paleomagnetism*, Fig. S3, and Table S6). Samples OLL-2, G02-B, and NL-13c already have published shallow magnetization directions similar to those reported for the Ongeluk Formation (6, 26, 27).

Discussion

The Ongeluk LIP. All samples were collected stratigraphically from within or below the lower Ongeluk Formation (Fig. 1) and represent either the feeder system of dolerite dikes and sills to the Ongeluk Formation basalts or coarse-grained interiors of thicker basalt flows. We interpret the Westerberg Sill Province and the N-trending dolerite dike swarm (Fig. 1), both intruding into the Griqualand West subbasin stratigraphy, as parts of the same short-lived magmatic event based on their temporal, spatial, and stratigraphic proximities and similar paleomagnetic results. The age of the Westerberg Sill itself was defined by an upper intercept date of 2,441 ± 6 Ma composed of five discordant baddeleyite analyses (28). However, excluding the most discordant analysis from this result yields a more probable upper intercept date of 2,428 ± 4 Ma. This reinterpretation is supported by concordant baddeleyite analyses from a second sill dated at 2,426 ± 1 Ma as part of the same study (28). Combining all of these dates, we calculate a weighted mean date of 2,425.5 ± 2.6 Ma (Fig. 2) as the age of a single relatively short-lived magmatic event, which is now clearly distinguished from ≤2,250–2,240 Ma Hekpoort Formation volcanism with which it was previously correlated. Because sample NL-13c is located ∼1,000 km to the east of the other sample sites, our results indicate a defined craton-scale LIP, the Ongeluk LIP.

The Ongeluk Key Paleomagnetic Pole. The VGPs presented in this study overlap with previously published paleopoles for the Ongeluk Formation and associated intrusions (6, 26–28). Collectively, the combined VGPs from all of these studies for the basalts from the Ongeluk Formation (6) and their intrusive feeders (26–28) define a grand key paleomagnetic pole for the Ongeluk LIP that is near-equatorial (29) at 4.1° N, 282.9° E (Table S7), with an A_{95} of 5.3° that achieves five of seven on the quality scale by Van der Voo (30).

Revising the Transvaal Supergroup Stratigraphy. The age for Ongeluk Formation volcanism demands the revision of stratigraphic correlations between the successions of the Griqualand West and Transvaal subbasins of the Transvaal Supergroup (Fig. 1). Previous studies have correlated the Postmasburg and Pretoria Groups using the 2,222 ± 13 Ma Ongeluk Formation and the ≤2,250–2,240 Ma Hekpoort Formation volcanic rocks (11, 12, 14, 18). This correlation is now shown to be incorrect based on the 2,426 ± 3 Ma age constraint provided by the Ongeluk Formation volcanic rocks and associated intrusions. In addition, lithologic and chemostratigraphic data for the Duitschland and Rooihoogte formations (15, 18, 23, 24, 31) coupled with recent age constraints (9, 11, 25) and arguments relying on basin architecture (16) indicate that the Duitschland and Rooihoogte formations are younger than the Postmasburg Group (Fig. 1). A more complete discussion on the Transvaal Supergroup stratigraphy and the proposed revisions is provided in the stratigraphic synthesis (*SI Methods*, *Stratigraphic Synthesis*).

Atmospheric Oxygen Oscillations. This stratigraphic interpretation indicates a dynamic state of atmospheric oxygen levels during the early Paleoproterozoic glacial period. The onset of the GOE occurred in the immediate aftermath of the Makganyene Formation glaciation with deposition of the world's largest manganese deposit, the Hotazel Formation, with a negative Ce anomaly, both indicative of oxygenation (7, 21). This oxygenation was followed by a return to anoxic atmospheric conditions as indicated by the lack of a Ce anomaly in foreslope carbonates of the Mooidraai Formation (Fig. 1) (21, 32) and a mass-independent fractionation of sulfur (MIF-S) signal recorded by early diagenetic sulfides from the lower Duitschland Formation (Fig. 1) (23). Subsequent oxygenation events occurred during deposition of the upper Duitschland Formation (23) and once again, in the middle of the Rooihoogte Formation (24) as indicated by the reappearance and disappearance of the MIF-S signal (Fig. 1).

Detrital pyrite grains persist above the oldest glacial diamictite in the Mississagi Formation in the Huronian Supergroup of the Superior Craton, Canada (33) and support oscillations in atmospheric oxygen herein inferred from the records of the Transvaal Supergroup (Fig. 3). Our geochronologic and stratigraphic framework argues against a simple, monotonic rise of atmospheric oxygen in the early Paleoproterozoic, a time period further characterized by four glaciations. Instead, the onset of the GOE was followed by oscillations in atmospheric oxygen content across the 10^{-5} present atmospheric level (PAL) threshold over an ∼200-My interval, adding empirical evidence to atmospheric modeling predictions (4).

Linking Snowball Earth and the GOE. The Makganyene Formation, deposited in the tropics (6), records the oldest known Snowball Earth event (7). Makganyene Formation diamictites are now constrained to be slightly older than ca. 2,426 Ma and likely correlate with glacial units of the Ramsay Lake Formation in the Huronian Supergroup, Canada and the Campbell Lake Formation from the Snowy Pass Supergroup on the Wyoming Craton in the United States. Other correlative glacial units worldwide include the ca. 2,435 Ma Polisarka Formation on the Kola–Karelia Craton in Fennoscandia (34) as well as possibly, the Meteorite Bore Member on the Pilbara Craton in Australia, defining the wide extent of the oldest Paleoproterozoic glaciation (Fig. 3). This early Paleoproterozoic glaciation is broadly coeval with the onset of the GOE; both events are now tightly bracketed between ca. 2,460 Ma, the age of volcanic rocks near the base of the Huronian Supergroup (8, 10), and ca. 2,426 Ma, the approximate age of the Makganyene Formation glaciation and near-coeval Ongeluk Formation volcanic rocks in the Transvaal Supergroup. In addition, the 2,442 ± 2 Ma Seidorechka Formation and the overlying 2,435 ± 2 Ma Polisarka formations (34, 35) overlying the Kola–Karelia Craton may tightly bracket the oldest Paleoproterozoic glacial event between ca. 2,442 Ma and 2,435 Ma, respectively, implying that it lasted less than 7 My (Fig. 3).

Our results add to the growing evidence for large low-latitude continental landmasses in the early Paleoproterozoic, including

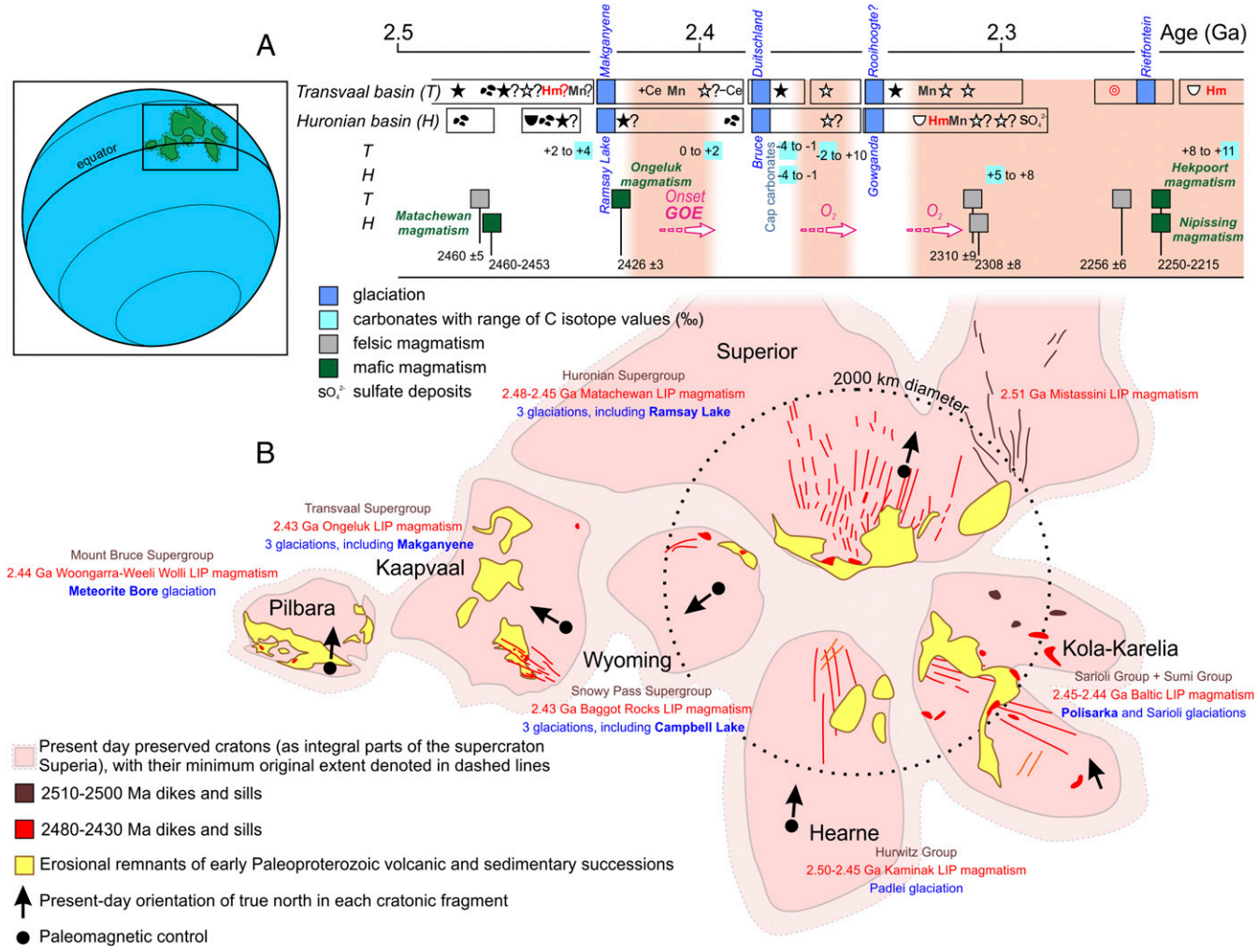

Fig. 3. *A* is a graph illustrating the approximate chronology (Table S1) of the glaciations and atmospheric oxygen oscillations according to the related redox indicators in the Huronian and Transvaal basins (Table S2) using the same symbols as used in Fig. 1. Also shown are dated mafic and felsic magmatic events as well as $\delta^{13}C$ ranges for carbonates (Tables S1 and S2) and the extent of stratigraphic records in each basin denoting gaps in records at unconformities and disconformities. (*B*) The early Paleoproterozoic geography of the Superior, Kola–Karelia, Hearne, and Wyoming cratons as integral parts of the supercraton Superia (5, 36)* with the addition of the Kaapvaal and Pilbara cratons in the supercraton Vaalbara configuration (52). The early Paleoproterozoic basins developed on these cratonic fragments include both ca. 2.51–2.43 Ga volcanic rocks and glacial units, which can be correlated across the cratons. The glacial units in bold denote the glacial deposits likely recording the first glaciation. All of the cratonic fragments also contain dolerite dikes and sills emplaced between ca. 2.51 Ga and 2.43 Ga, showing the extent of the LIPs formed during this time. Available paleomagnetic studies indicate that the majority of the cratonic fragments (as part of supercraton Superia) were positioned near the paleoequator. The arrows denoting present-day true north in the crustal blocks illustrate the rotations necessary to make the reconstruction. (*Inset*) The hypothesized paleolatitude of these Archean cratons in the early Paleoproterozoic.

the Kaapvaal Craton (6) and the clan of cratons that defines supercraton Superia (5, 36, 37): Superior, Wyoming, Hearne, and Karelia–Kola. These landmasses, at least in part contiguous, record a series of LIP events between 2,510 Ma and 2,440 Ma and include the Mistassini, Kaminak, Baltic, Baggot Rocks, and Matachewan LIPs (Fig. 3) (5) before the ca. 2,426 Ma Ongeluk LIP of the Kaapvaal Craton. Cumulatively, these large juvenile volcanic provinces on extensive low-latitude continental landmasses are likely to have triggered near-equatorial glaciations via enhanced chemical weathering of aerially extensive, nutrient-rich continental flood basalts. This weathering resulted in increased carbon dioxide drawdown (38, 39) and an enhanced flux of phosphorus and other essential nutrients (40) onto extensive continental margins and into intracratonic basins. An enhanced nutrient flux would have greatly increased photosynthetic activity and oxygen production, temporally linked to higher net burial of organic carbon in accumulating sediments, as reflected by $\delta^{13}C$ values of carbonates in the upper Tongwane Formation of the Transvaal Supergroup (31). The Tongwane Formation is locally preserved above the ca. 2,480–2,460 Ma iron formations (41) but below the major unconformity documented in the entire Transvaal basin (Fig. 1) (18). Thus, even an incipient rise of free atmospheric oxygen would have led to rapid oxidation of atmospheric methane (42), forcing catastrophic climate change and plunging Earth into a global glaciation (43). Importantly, the dated near-equatorial Ongeluk LIP, conformably overlying and interfingering with the uppermost Makganyene Formation glacial diamictites (Fig. 1), illustrates the dual role of LIPs in these global events, in that they would also have contributed carbon dioxide to rebuilding the greenhouse atmosphere that led to abrupt termination of the first Snowball Earth state of the early Paleoproterozoic.

*Bleeker W, Chamberlain K, Kamo S, Kilian T, Buchan K (2016) Kaapvaal, Superior and Wyoming: Nearest neighbours in supercraton Superia. Proceedings of the 35th International Geological Congress.

Comparing the Paleoproterozoic with the Neoproterozoic. In the Neoproterozoic, a remarkably similar sequence of events occurred, involving successive emplacement of multiple LIPs on the supercontinent Rodinia, a low-latitude position of this supercontinent, and incipient rifting and breakup (44). The massive Franklin LIP at ca. 717 Ma (45) immediately preceded the most dramatic and longest global glaciation of the Neoproterozoic, the Sturtian (46). This overall period is characterized by the second most dramatic change in surface redox conditions linked with Snowball Earth glaciations (47) and accompanied high rates of organic carbon burial (48, 49). Although substantial differences between the Paleo- and Neoproterozoic glacial periods might be expected, for instance, in the triggering mechanisms for the initial global glaciations, because methane was probably a more important greenhouse gas before the Makganyene glaciation (42, 43) than before the Sturtian glaciation (38, 39), there are also uncanny parallels. Examples include supercraton- or supercontinent-size continental landmasses that were capped by continental flood basalts, incipient rifting and/or breakup, and rapid transit to low latitudes. All of these factors enhanced chemical weathering of juvenile basaltic material and greatly increased the flux of biolimiting nutrients to depositional basins, thus leading to a biotic response of higher organic carbon burial (40, 50) as well as deposition of giant iron and manganese deposits. It seems likely that these similar scenarios are not coincidental but that the critical factors (assembly of large landmasses, LIPs, incipient rifting, and relief enhancement—all resulting in a lithospheric mass anomaly and movement to low latitudes, high rates of organic carbon burial, surface oxygenation, and Snowball Earth glaciations) are mechanistically linked. In this case, a critical link might be true polar wander caused by the lithospheric mass anomaly that nudged the basalt-covered and rifting supercontinental landmasses to the equator (51), where chemical weathering and nutrient fluxes kicked into high gear and triggered the biotic, redox, and climatic responses.

Methods

Sampling. Samples in this study were taken from dolerite intrusions that intruded into the basement of the Kaapvaal Craton and the overlying cover succession of the Transvaal Supergroup in the Griqualand West subbasin, South Africa, except for one sample taken ~1,000 km to the east (Fig. 1, *SI Methods*, Fig. S1, and Table S3). One sample is tentatively interpreted as a coarse-grained basalt from the base of the Ongeluk Formation.

Geochronology—ID-TIMS Analysis. Water-based separation of baddeleyite was attempted for all rock samples at Lund University. Samples NL-13c and G02-B yielded baddeleyite grains using this method. Grains were selected and analyzed using U-Pb ID-TIMS on a Thermo Finnigan Triton Mass Spectrometer at the Department of Geosciences at the Swedish Museum of Natural History. Additional details of the operating procedures for the ID-TIMS analyses at the Swedish Museum of Natural History and results are given in *SI Methods*, Fig. S2, and Table S4.

Geochronology—SIMS Analysis. Zr-bearing phases were imaged, mapped using SEM in conjunction with energy-dispersive spectrometry in samples TGS-05 and OLL-2, and then, ranked (*SI Methods* and Fig. S2). U-Pb isotopic data using SIMS were determined in situ on the microbaddeleyite grains in the mapped thin sections using the CAMECA ims1270 Mass Spectrometer at the University of California, Los Angeles (UCLA). Additional details of the operating procedures for the SIMS at UCLA and results are given in *SI Methods*, Fig. S2, and Table S5.

Paleomagnetism. Measurements of magnetic remanence from samples TGS-05 and MDK-05 were made using the superconducting vertical 2G Enterprises DC-4K Rock Magnetometer at the University of Johannesburg (UJ). All specimens were exposed to stepwise alternating-field demagnetization. Additional details of the sampling and operating procedures for the magnetometer at the UJ and results are given in *SI Methods*, Fig. S3, and Table S6.

ACKNOWLEDGMENTS. We thank the staff of the SIMS and the TIMS laboratories at UCLA and the Department of Geosciences, Swedish Museum of Natural History, respectively, for all of the assistance during analyses. We thank N. Beukes for providing sample TGS-05. Funding was provided by grants from the Royal Physiographic Society in Lund (A.P.G.) and the Swedish Research Council (U.S.); M.O.d.K. and A.B. acknowledge support from the South African Department of Science and Technology and the National Research Foundation (DST-NRF)–funded Centre of Excellence for Integrated Mineral and Energy Resource Analysis (CIMERA). This article is a contribution to International Geoscience Programme (IGCP) 648: Supercontinents and Global Geodynamics.

1. Holland HD (2002) Volcanic gases, black smokers, and the Great Oxidation Event. *Geochim Cosmochim Acta* 66(21):3811–3826.
2. Hoffman PF (2013) The Great Oxidation and a Siderian snowball Earth: MIF-S based correlation of Paleoproterozoic glacial epochs. *Chem Geol* 362:143–156.
3. Goldblatt C, Lenton TM, Watson AJ (2006) Bistability of atmospheric oxygen and the Great Oxidation. *Nature* 443(7112):683–686.
4. Daines SJ, Lenton TM (2016) The effect of widespread early aerobic marine ecosystems on methane cycling and the Great Oxidation. *Earth Planet Sci Lett* 434:42–51.
5. Ernst R, Bleeker W (2010) Large igneous provinces (LIPs), giant dyke swarms, and mantle plumes: Significance for breakup events within Canada and adjacent regions from 2.5 Ga to the Present. *Can J Earth Sci* 47(5):695–739.
6. Evans DA, Beukes NJ, Kirschvink JL (1997) Low-latitude glaciation in the Palaeoproterozoic era. *Nature* 386(6622):262–266.
7. Kirschvink JL, et al. (2000) Paleoproterozoic snowball earth: Extreme climatic and geochemical global change and its biological consequences. *Proc Natl Acad Sci USA* 97(4):1400–1405.
8. Ketchum KY, Heaman LM, Bennett G, Hughes DJ (2013) Age, petrogenesis and tectonic setting of the Thessalon volcanic rocks, Huronian Supergroup, Canada. *Precambrian Res* 233:144–172.
9. Rasmussen B, Bekker A, Fletcher IR (2013) Correlation of Paleoproterozoic glaciations based on U-Pb zircon ages for tuff beds in the Transvaal and Huronian Supergroups. *Earth Planet Sci Lett* 382:173–180.
10. Bleeker W, Kamo SL, Ames DE, Davis D (2015) New field observations and U-Pb ages in the Sudbury area: Toward a detailed cross-section through the deformed Sudbury Structure. *Geol Surv Canada Open File* 7856:151–166.
11. Schröder S, Beukes NJ, Armstrong RA (2016) Detrital zircon constraints on the tectonostratigraphy of the Paleoproterozoic Pretoria Group, South Africa. *Precambrian Res* 278:362–393.
12. Beukes NJ, Dorland H, Gutzmer J, Nedachi M, Ohmoto H (2002) Tropical laterites, life on land, and the history of atmospheric oxygen in the Paleoproterozoic. *Geology* 30(6):491–494.
13. Eriksson PG, Cheney ES (1992) Evidence for the transition to an oxygen-rich atmosphere during the evolution of red beds in the lower Proterozoic sequences of southern Africa. *Precambrian Res* 54(2-4):257–269.
14. Cornell DH, Schütte SS, Eglington BL (1996) The Ongeluk basaltic andesite formation in Griqualand West, South Africa: Submarine alteration in a 2222 Ma Proterozoic sea. *Precambrian Res* 79(1-2):101–123.
15. Bau M, Romer RL, Lüders V, Beukes NJ (1999) Pb, O, and C isotopes in silicified Mooidraai dolomite (Transvaal Supergroup, South Africa): Implications for the composition of Paleoproterozoic seawater and "dating" the increase of oxygen in the Precambrian atmosphere. *Earth Planet Sci Lett* 174(1-2):43–57.
16. Moore JM, Tsikos H, Polteau S (2001) Deconstructing the Transvaal Supergroup, South Africa: Implications for Palaeoproterozoic palaeoclimate models. *J Afr Earth Sci* 33(3-4):437–444.
17. Polteau S, Moore JM, Tsikos H (2006) The geology and geochemistry of the Palaeoproterozoic Makganyene diamictite. *Precambrian Res* 148(3-4):257–274.
18. Eriksson PG, Altermann W, Hartzer FJ (2006) The Transvaal Supergroup. *The Geology of South Africa*, eds Johnson MJ, Anhaeusser CR, Thomas RJ (Geological Society of South Africa/Council for Geoscience, Johannesburg), pp 237–260.
19. Moore JM, Polteau S, Armstrong RA, Corfu F, Tsikos H (2012) The age and correlation of the Postmasburg Group, southern Africa: Constraints from detrital zircon grains. *J Afr Earth Sci* 64:9–19.
20. Fairey B, Tsikos H, Corfu F, Polteau S (2013) U-Pb systematics in carbonates of the Postmasburg Group, Transvaal Supergroup, South Africa: Primary versus metasomatic controls. *Precambrian Res* 231:194–205.
21. Bau M, Alexander B (2006) Preservation of primary REE patterns without Ce anomaly during dolomitization of Mid-Paleoproterozoic limestone and the potential re-establishment of marine anoxia immediately after the "Great Oxidation Event." *South Afr J Geol* 109(1-2):81–86.
22. Johnson JE, Gerpheide A, Lamb MP, Fischer WW (2014) O_2 constraints from Paleoproterozoic detrital pyrite and uraninite. *Geol Soc Am Bull* 126(5-6):813–830.
23. Guo Q, et al. (2009) Reconstructing Earth's surface oxidation across the Archean-Proterozoic transition. *Geology* 37(5):399–402.
24. Luo G, et al. (2016) Rapid oxygenation of Earth's atmosphere 2.33 billion years ago. *Sci Adv* 2(5):e1600134.
25. Hannah JL, Bekker A, Stein HJ, Markey RJ, Holland HD (2004) Primitive Os and 2316 Ma age for marine shale: Implications for Paleoproterozoic glacial events and the rise of atmospheric oxygen. *Earth Planet Sci Lett* 225:43–52.
26. de Kock MO, et al. (2009) Paleomagnetism of a Neoarchean-Paleoproterozoic carbonate ramp and carbonate platform succession (Transvaal Supergroup) from surface outcrop and drill core, Griqualand West region, South Africa. *Precambrian Res* 169(1-2):80–99.
27. Lubnina N, Ernst R, Klausen M, Söderlund U (2010) Paleomagnetic study of NeoArchean-Paleoproterozoic dykes in the Kaapvaal Craton. *Precambrian Res* 183(3):523–552.
28. Kampmann TC, Gumsley AP, de Kock MO, Söderlund U (2015) U-Pb geochronology and paleomagnetism of the Westerberg Sill Suite, Kaapvaal Craton - Support for a

coherent Kaapvaal-Pilbara Block (Vaalbara) into the Paleoproterozoic? *Precambrian Res* 269:58–72.
29. Buchan KL (2013) Key paleomagnetic poles and their use in Proterozoic continent and supercontinent reconstructions: A review. *Precambrian Res* 238:93–110.
30. Van der Voo R (1990) The reliability of paleomagnetic data. *Tectonophysics* 184(1):1–9.
31. Bekker A, et al. (2001) Chemostratigraphy of the Paleoproterozoic Duitschland Formation, South Africa: Implications for coupled climate change and carbon cycling. *Am J Sci* 301(3):261–285.
32. Kunzmann M, Gutzmer J, Beukes NJ, Halverson GP (2014) Depositional environment and lithostratigraphy of the Paleoproterozoic Mooidraai Formation, Kalahari Manganese Field, South Africa. *South Afr J Geol* 117(2):173–192.
33. Ulrich T, Long DGF, Kamber BS, Whitehouse MJ (2011) In situ trace element and sulfur isotope analysis of pyrite in a Paleoproterozoic Gold Placer Deposit, Pardo and Clement Townships, Ontario, Canada. *Econ Geol* 106(4):667–686.
34. Brasier AT, et al. (2013) Earth's earliest global glaciation? Carbonate geochemistry and geochronology of the Polisarka Sedimentary Formation, Kola Peninsula, Russia. *Precambrian Res* 235:278–294.
35. Amelin YV, Heaman LM, Semenov VS (1995) U-Pb geochronology of layered mafic intrusions in the eastern Baltic Shield: Implications for the timing and duration of Paleoproterozoic continental rifting. *Precambrian Res* 75(1-2):31–46.
36. Bleeker W, Ernst R (2006) Short-lived mantle generated magmatic events and their dyke swarms: The key unlocking Earth's paleogeographic record back to 2.6 Ga. *Dyke Swarms—Time Markers of Crustal Evolution*, eds Hanski E, Mertanen S, Rämö T, Vuollo J (Taylor and Francis, London), pp 3–26.
37. Bleeker W (2003) The late Archean record: A puzzle in ca. 35 pieces. *Lithos* 71(2-4):99–134.
38. Marshall HG, Walker JCG, Kuhn WR (1988) Long-term climate change and the geochemical cycle of carbon. *J Geophys Res Atmos* 93(D1):791–801.
39. Donnadieu Y, Goddéris Y, Ramstein G, Nédélec A, Meert J (2004) A 'snowball Earth' climate triggered by continental break-up through changes in runoff. *Nature* 428(6980):303–306.
40. Horton F (2015) Did phosphorus derived from the weathering of large igneous provinces fertilize the Neoproterozoic ocean? *Geochem Geophys Geosyst* 16(6):1723–1738.
41. Schröder S, Warke MR (2016) Termination of BIF deposition in the Paleoproterozoic: The Tongwane Formation, South Africa. *South Afr J Geol* 119(2):329–346.
42. Pavlov AA, Kasting JF (2002) Mass-independent fractionation of sulfur isotopes in Archean sediments: Strong evidence for an anoxic Archean atmosphere. *Astrobiology* 2(1):27–41.
43. Bekker A, Kaufman AJ (2007) Oxidative forcing of global climate change: A biogeochemical record across the oldest Paleoproterozoic ice age in North America. *Earth Planet Sci Lett* 258(3-4):486–499.
44. Li ZX, et al. (2008) Assembly, configuration, and break-up history of Rodinia: A synthesis. *Precambrian Res* 160(1-2):179–210.
45. Macdonald FA, et al. (2010) Calibrating the Cryogenian. *Science* 327(5970):1241–1243.
46. Rooney AD, Strauss JV, Brandon AD, Macdonald FA (2015) A Cryogenian chronology: Two long-lasting synchronous Neoproterozoic glaciations. *Geology* 43(5):459–462.
47. Pogge von Strandmann PAE, et al. (2015) Selenium isotope evidence for progressive oxidation of the Neoproterozoic biosphere. *Nat Commun* 6:10157.
48. Thomson D, Rainbird RH, Planavsky NJ, Lyons TW, Bekker A (2015) Chemostratigraphy of the Shaler Supergroup, Victoria Island, NW Canada: A record of ocean composition prior to the Cryogenian glaciations. *Precambrian Res* 263:232–245.
49. Turner EC, Bekker A (2016) Thick sulfate evaporite accumulations marking a mid-Neoproterozoic oxygenation event (Ten Stone Formation, Northwest Territories, Canada). *Geol Soc Am Bull* 128(1-2):203–222.
50. Cox GM, et al. (2016) Continental flood basalt weathering as a trigger for Neoproterozoic Snowball Earth. *Earth Planet Sci Lett* 446:89–99.
51. Li Z-X, Zhong S (2009) Supercontinent-superplume coupling, true polar wander and plume mobility: Plate dominance in whole-mantle tectonics. *Phys Earth Planet Inter* 176(3-4):143–156.
52. de Kock MO, Evans DAD, Beukes NJ (2009) Validating the existence of Vaalbara in the Neoarchean. *Precambrian Res* 174(1-2):145–154.
53. Gumsley A, et al. (2015) Precise U-Pb baddeleyite age dating of the Usushwana Complex, southern Africa: Implications for the Mesoarchaean magmatic and sedimentological evolution of the Pongola Supergroup, Kaapvaal Craton. *Precambrian Res* 267:174–185.
54. Stacey JS, Kramers JD (1975) Approximation of terrestrial lead isotope evolution by a two-stage model. *Earth Planet Sci Lett* 26(2):207–221.
55. Jaffey AH, Flynn KF, Glendenin LE, Bentley WC, Essling AM (1971) Precision measurement of half-lives and specific activities of U235 and U238. *Phys Rev C Nucl Phys* 4:1889–1906.
56. Steiger RH, Jäger E (1977) Subcommission on geochronology: Convention on the use of decay constants in geo- and cosmochronology. *Earth Planet Sci Lett* 36(3):359–362.
57. Ludwig KR (2003) *User's Manual for Isoplot 3.00—A Geochronological Toolkit for Microsoft Excel* (Berkeley Geochronology Center, Berkeley, CA), Special Publ 4.
58. Chamberlain KR, et al. (2010) In situ U-Pb SIMS (IN-SIMS) micro-baddeleyite dating of mafic rocks: Method with examples. *Precambrian Res* 183(3):379–387.
59. Compston W, Williams IS, Meyer C (1984) U-Pb geochronology of zircons form lunar Breccia 73217 using a sensitive high mass-resolution ion microprobe. *J Geophys Res Solid Earth* 89(S02):B525–B534.
60. Ireland TR, Williams IS (2003) Considerations in zircon geochronology by SIMS. *Rev Miner Geochem* 53(1):215–241.
61. Kirschvink JL (1980) The least-squares line and plane and the analysis of paleomagnetic data. *Geophys J Int* 62(3):699–718.
62. Jones CH (2002) User-driven integrated software lives: "Paleomag" paleomagnetics analysis on the Macintosh. *Comput Geosci* 28(10):1145–1151.
63. Williams SE, Müller RD, Landgrebe TCW, Whittaker JM (2012) An open-source software environment for visualizing and refining plate tectonic reconstructions using high-resolution geological and geophysical data sets. *GSA Today* 22(4):4–9.
64. Evans DAD, Beukes NJ, Kirschvink JL (2002) Paleomagnetism of a lateritic paleoweathering horizon and overlying Paleoproterozoic red beds from South Africa: Implications for the Kaapvaal apparent polar wander path and a confirmation of atmospheric oxygen enrichment. *J Geophys Res Solid Earth* 107(B12):EPM 2-1–EPM 2-22.
65. Schröder S, Bedorf D, Beukes NJ, Gutzmer J (2011) From BIF to red beds: Sedimentology and sequence stratigraphy of the Paleoproterozoic Koegas Subgroup (South Africa). *Sediment Geol* 236(1-2):25–44.
66. Beukes NJ (1984) Sedimentology of the Kuruman and Griquatown iron-formations, Transvaal Supergroup, Griqualand West, South Africa. *Precambrian Res* 24(1):47–84.
67. Bekker A, et al. (2008) Fractionation between inorganic and organic carbon during the Lomagundi (2.22–2.1 Ga) carbon isotope excursion. *Earth Planet Sci Lett* 271(1-4):278–291.
68. Coetzee LL, Beukes NJ, Gutzmer J, Kakegawa T (2006) Links of organic carbon cycling and burial to depositional depth gradients and establishment of a snowball Earth at 2.3 Ga. Evidence from the Timeball Hill Formation,Transvaal Supergroup, South Africa. *South Afr J Geol* 109(1-2):109–122.
69. Farquhar J, Bao H, Thiemens M (2000) Atmospheric influence of Earth's earliest sulfur cycle. *Science* 289(5480):756–759.
70. Bekker A, et al. (2004) Dating the rise of atmospheric oxygen. *Nature* 427(6970):117–120.
71. Johnson JE, et al. (2013) Manganese-oxidizing photosynthesis before the rise of cyanobacteria. *Proc Natl Acad Sci USA* 110(28):11238–11243.
72. Pickard AL (2003) SHRIMP U-Pb zircon ages for the Palaeoproterozoic Kuruman Iron Formation, northern Cape Province, South Africa: Evidence for simultaneous BIF deposition on Kaapvaal and Pilbara cratons. *Precambrian Res* 125(3-4):275–315.
73. Sumner DY, Bowring SA (1996) U-Pb geochronologic constraints on deposition of the Campbellrand Subgroup, Transvaal Supergroup, South Africa. *Precambrian Res* 79(1-2): 25–35.
74. Barton ES, Altermann W, Williams IS, Smith CB (1994) U-Pb zircon age for a tuff in the Campbell Group, Griqualand West sequence, South Africa: Implications for early Proterozoic rock accumulation rates. *Geology* 22(4):343–346.
75. Altermann W, Nelson DR (1998) Sedimentation rates, basin analysis and regional correlations of three Neoarchaean and Palaeoproterozoic sub-basins of the Kaapvaal craton as inferred from precise U-Pb zircon ages from volcaniclastic sediments. *Sediment Geol* 120(1-4):225–256.
76. Nelson DR, Trendall AF, Altermann W (1999) Chronological correlations between the Pilbara and Kaapvaal cratons. *Precambrian Res* 97(3-4):165–189.
77. Swart QD (1999) *Carbonate Rocks of the Paleoproterozoic Pretoria and Postmasburg Groups, Transvaal Supergroup* (Rand Afrikaans Univ, Johannesburg).
78. Bekker A, Karhu JA, Kaufman AJ (2006) Carbon isotope record for the onset of the Lomagundi carbon isotope excursion in the Great Lakes area, North America. *Precambrian Res* 148(1-2):145–180.
79. Sekine Y, et al. (2011) Manganese enrichment in the Gowganda Formation of the Huronian Supergroup: A highly oxidizing shallow-marine environment after the last Huronian glaciation. *Earth Planet Sci Lett* 307(1-2):201–210.
80. Chandler FW (1988) Diagenesis of sabkha-related, sulphate nodules in the early Proterozoic Gordon Lake formation, Ontario, Canada. *Carbonates Evaporites* 3(1):75–94.
81. Fedo CM, Nesbitt HW, Young GM (1995) Unraveling the effects of potassium metasomatism in sedimentary rocks and paleosols, with implications for paleoweathering conditions and provenance. *Geology* 23(10):921–924.
82. Papineau D, Mojzsis SJ, Schmitt AK (2007) Multiple sulfur isotopes from Paleoproterozoic Huronian interglacial sediments and the rise of atmospheric oxygen. *Earth Planet Sci Lett* 255(1-2):188–212.
83. Bekker A, Kaufman AJ, Karhu JA, Eriksson KA (2005) Evidence for Paleoproterozoic cap carbonates in North America. *Precambrian Res* 137(3-4):167–206.
84. Murakami T, Utsunomiya S, Imazu Y, Prasad N (2001) Direct evidence of late Archean to early Proterozoic anoxic atmosphere from a product of 2.5 Ga old weathering. *Earth Planet Sci Lett* 184(2):523–528.
85. Roscoe SM (1969) Huronian rocks and uraniferous conglomerates in the Canadian Shield. *Geol Surv Canada Open File* 68:1–205.
86. Gumsley A, Rådman J, Söderlund U, Klausen M (2016) U–Pb baddeleyite geochronology and geochemistry of the White Mfolozi Dyke Swarm: Unravelling the complexities of 2.70–2.66 Ga dyke swarms across the eastern Kaapvaal Craton, South Africa. *GFF* 138(1):115–132.
87. Reischmann T (1995) Precise U/Pb age determination with baddeleyite (ZrO2), a case study from the Phalaborwa igneous complex, South Africa. *South Afr J Geol* 98(1):1–14.
88. Letts S, Torsvik TH, Webb SJ, Ashwal LD (2011) New Palaeoproterozoic palaeomagnetic data from the Kaapvaal Craton, South Africa. *Geol Soc Lond Spec Publ* 357:9–26.
89. Zeh A, Ovtcharova M, Wilson AH, Schaltegger U (2015) The Bushveld Complex was emplaced and cooled in less than one million years—results of zirconology, and geotectonic implications. *Earth Planet Sci Lett* 418:103–114.
90. Letts S, Torsvik TH, Webb SJ, Ashwal LD (2009) Palaeomagnetism of the 2054 Ma Bushveld Complex (South Africa): Implications for emplacement and cooling. *Geophys J Int* 179(2):850–872.
91. Dorland HC, Beukes NJ, Gutzmer J, Evans DAD, Armstrong RA (2006) Precise SHRIMP U-Pb zircon age constraints on the lower Waterberg and Soutpansberg Groups, South Africa. *South Afr J Geol* 109(1-2):139–156.
92. de Kock MO, Evans DAD, Dorland HC, Beukes NJ, Gutzmer J (2006) Paleomagnetism of the lower two unconformity-bounded sequences of the Waterberg Group, South Africa: Towards a better-defined apparent polar wander path for the Paleoproterozoic Kaapvaal Craton. *South Afr J Geol* 109(1-2):157–182.
93. Kamo SL, Reimold WU, Krogh TE, Colliston WP (1996) A 2.023 Ga age for the Vredefort impact event and a first report of shock metamorphosed zircons in pseudotachylitic breccias and Granophyre. *Earth Planet Sci Lett* 144(3-4):369–387.
94. Carporzen L, Gilder SA, Hart RJ (2005) Palaeomagnetism of the Vredefort meteorite crater and implications for craters on Mars. *Nature* 435(7039):198–201.